Supporting Information

Efficient and thermally stable broadband near-infrared emitting from near zero thermal expansion $AlP_3O_9:Cr^{3+}$ phosphor

Decai Huang[a,b], Xianguo He[a,b], Jingrong Zhang[a,b], Jie Hu[a,b], Sisi Liang[a,b], Dejian Chen[a,b], Kunyuan Xu[a,b], and Haomiao Zhu[a,b,c,*]

[a] *CAS Key Laboratory of Design and Assembly of Functional Nanostructures, Fujian Key Laboratory of Nanomaterials, Fujian Institute of Research on the Structure of Matter, Chinese Academy of Sciences, Fuzhou, Fujian, 350002, China.*

[b] *Xiamen Key Laboratory of Rare Earth Photoelectric Functional Materials, Xiamen Research Center of Rare Earth Materials, Haixi Institute, Chinese Academy of Sciences, Xiamen, Fujian, 361021, China.*

[c] *Ganjiang Innovation Academy, Chinese Academy of Sciences, Ganzhou, Jiangxi, 341000, China.*

E-mail: zhm@fjirsm.ac.cn

Supplementary Discussion: The D_q parameter is obtained from the peak energy of the $^4A_2 \rightarrow {}^4T_2$ transition, while Racah parameters *B* and *C* can be estimated by the following equations:[1]

$$E({}^4T_2 - {}^4A_2) = 10D_q \quad (1)$$

$$\frac{B}{D_q} = \frac{(\Delta E/D_q)^2 - 10(\Delta E/D_q)}{15(\Delta E/D_q - 8)} \quad (2)$$

$$3.05C = E({}^2E) - 7.9B + 1.8B^2/\Delta E \quad (3)$$

where $\Delta E = [E({}^4T_1) - E({}^4T_2)]$ is the difference between the energies of the $^4T_1$ and $^4T_2$ states and $E({}^2E)$ is the energy of the ^2E state. The value of $^4T_1$, $^4T_2$ and ^2E are estimated to be 20810, 14010 and 14780 cm^{-1} from the excitation and emission bands, respectively. Based on equations (1) – (3), the values of *B*, *C* and D_q/B were calculated to be 741 cm^{-1}, 3157 cm^{-1} and 1.89, respectively.

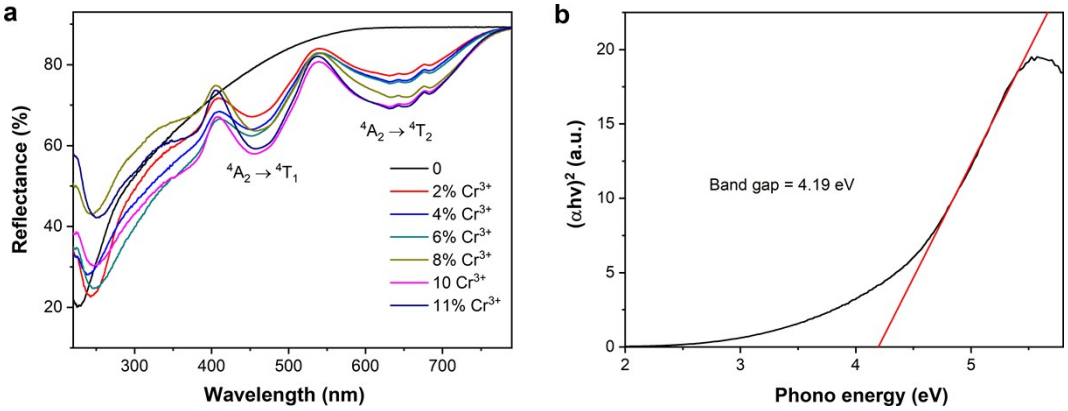

Fig. S1. (a) The diffuse reflectance spectra of the AlP_3O_9:xCr^{3+} (x = 0–11.0 at.%) samples. (b) The band gap simulation of the AlP_3O_9 crystal. The plot of $(\alpha hv)^2$ *vs* $(hv - E_g)$ is used to estimate the bandgap scale, α originates from the Kubelka-Munk function and $\alpha = (1 - R)^2/(2R)$, where R is the reflectivity value, hv is the photon energy, and E_g is the optical bandgap.[2]

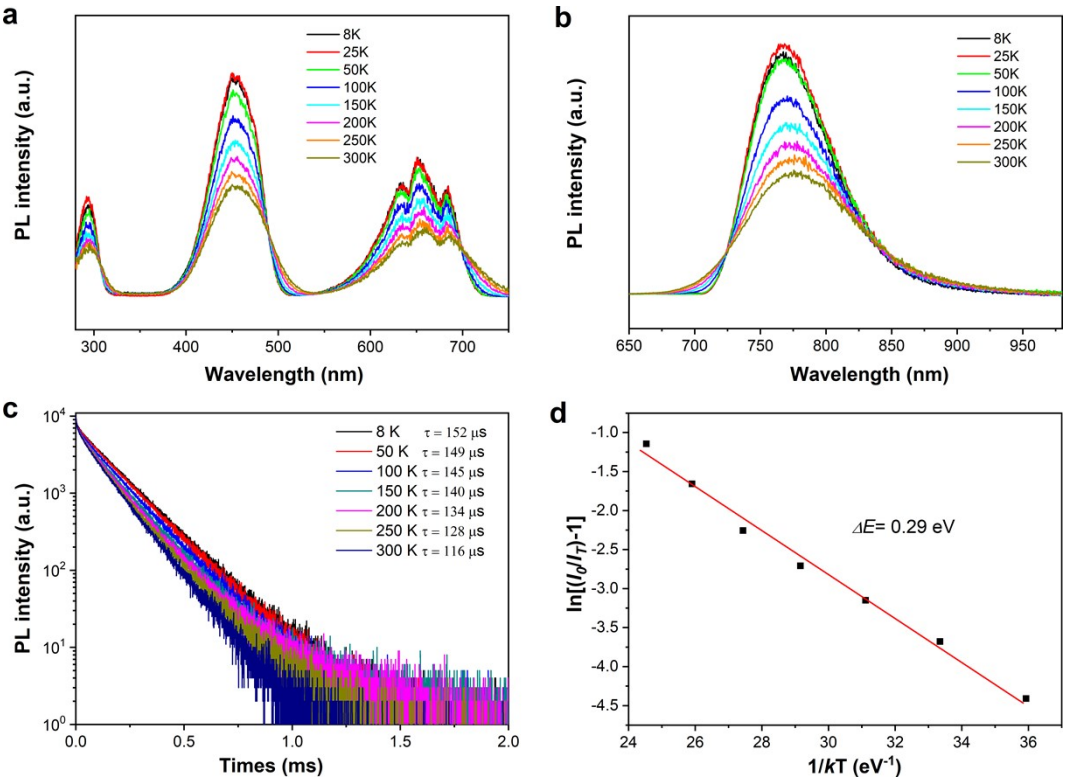

Fig. S2. (a) Excitation (λ_{em} = 780 nm) and (b) emission (λ_{ex} = 450 nm) spectra of the AlP_3O_9:6%Cr^{3+} sample measured at 8–300 K. (c) PL decay curves of the AlP_3O_9:6%Cr^{3+} sample measured by monitoring emission at 780 nm at 300–473 K. (d) The functional relationship of $\ln[(I_0/I_T)-1]$ versus $1/\kappa T$ of AlP_3O_9:6%Cr^{3+}.

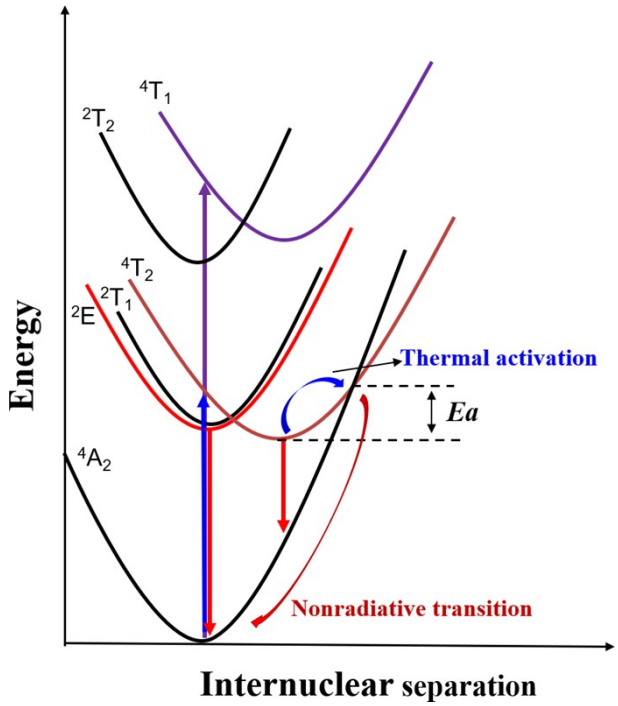

Fig. S3 Configurational coordinate diagram of Cr^{3+} ions in AlP_3O_9

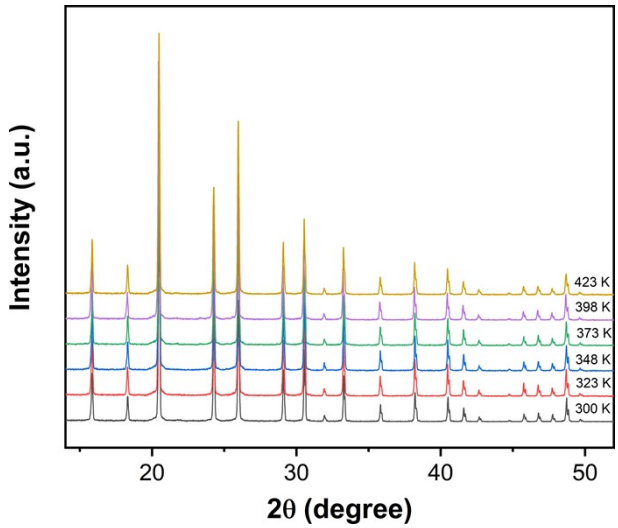

Fig. S4. The in-situ variable-temperature XRD patterns of the AlP_3O_9:6%Cr^{3+} sample at 300–423 K.

Table S1. Several key optical parameters of Cr^{3+}-activated phosphors.

Formula	AlP_3O_9:6%Cr
Crystal system	Cubic
Space group	$I\bar{4}3d$
$a = b = c$(Å)	13.73(6)
V(Å^3)	2591.86
$\alpha = \beta = \gamma$(°)	90
R_p(%)	8.45
R_{wp}(%)	6.86
χ^2	1.47

Table S2. The atom positions, fraction factors and thermal vibration parameters of the AlP_3O_9:6%Cr^{3+} sample.

Atom	*x*	*y*	*z*	Occupancy	Uiso (*100)
Al1	0.10560(6)	0.10560(6)	0.10560(6)	0.9400	0.452
Cr1	0.07132(7)	0.07132(7)	0.07132(7)	0.0600	4.594
P1	0.33037(3)	0.04785(2)	0.11910(6)	1.0000	2.130
O1	0.09114(2)	0.10094(5)	0.81502(4)	1.0000	2.535
O1	0.07518(1)	0.15059(0)	0.23271(3)	1.0000	2.310
O1	0.13658(9)	0.05964(9)	0.98029(3)	1.0000	2.228

Table S3. Internal and external PL QY and absorption efficiency at room temperature for $AlP_3O_9:Cr^{3+}$ samples with different Cr^{3+} doping concentrations.

Cr^{3+} (at.%)	1	2	3	4	5	6	7	8	10	11
IQY (%)	74	73	75	76	74	75	70	66	60	52
EQY (%)	25	26	29	32	33	36	35	34	32	29
Abs. (%)	34	36	39	42	45	48	50	51	54	56

Table S4. Several key optical parameters of Cr^{3+}-activated phosphors (Peak position > 780 nm).

Phosphor	Emission rang (nm)	Peak position (nm)	PL IQY (%)	$I_{423\,k}/I_{298\,k}$ (%)	Ref.
$AlP_3O_9:Cr^{3+}$	650-1000	780	76	91	This work
$ScBO_3:Cr^{3+}$	680-1000	780	72	~50	[3, 4]
$Li2MgZrO_4:Cr^{3+}$	650-1200	805	56	30	[5]
$Ga_{2-x}In(Sc)xO_3:Cr^{3+}$	650-1100	800	88-99	77	[6, 7]
$Sr_9M_{1-x}(PO_4)_7: Cr^{3+}$	700-1100	850	74	15	[8]
$GaTaO_4: Cr^{3+}$	700-1100	825	57	50	[9]
$ScF_6:Cr^{3+}$	700-1100	853	45	86	[10]
$LiInSi_2O_6:Cr^{3+}$	700-1100	840	75	77	[11]
$LiIn_2SbO_6:Cr^{3+}$	700-1300	960	7	~8	[12, 13]
$LiIn_2GeO_6:Cr^{3+}$	700-1200	880	81	~25	[14]
$LiGaP_2O_7: Cr^{3+}$	700-1200	846	~47	~15	[15]
$LiScP_2O_7: Cr^{3+}$	750-1100	880	74	20	[16]
$NaScGe_2O_6: Cr^{3+}$	700-1300	895	40	~50	[17]
$Mg_2GeO_4: Cr^{3+}$	700-1100	900	~48	~20	[18]
$LaSc_2B_4O_{12}: Cr^{3+}$	700-1150	870	52	~55	[19]
$Cs_2AgInCl_6: Cr^{3+}$	800-1400	1010	~22	~10	[20]
$Ca_3Hf_2Al_2SiO_{12}: Cr^{3+}$	650-1100	785	~75	~40	[21]
$La_3Ga_5GeO_{14}:Cr^{3+}$	700-1300	850	35	~60	[22, 23]
$La_2MgZrO_6:Cr^{3+}$	650-1200	825	~58	~30	[24]
$BaZrGe_3O_9:Cr^{3+}$	650-1200	830	-	53	[25]

Table S5. Interatomic distances and bond angles for AlP_3O_9:6%Cr^{3+} samples at 300 K and 423 K.

Distances (Å)	300 K	423 K	Variation ratio (%)	Bond angle (°)	300 K	423 K	Variation ratio (%)
Al1-O2	1.812(7)	1.818(1)	0.29	O2-Al1-O2	88.56(6)	88.91(2)	0.39
Al1-O3	1.801(5)	1.807(4)	0.32	O3-Al1-O3	88.62(4)	88.95(2)	0.37
Cr1-O2	1.899(2)	1.904(8)	0.29	O2-Cr1-O2	90.91(3)	91.19(7)	0.31
Cr1-O3	1.882(6)	1.888(2)	0.30	O3-Cr1-O3	91.92(1)	92.24(5)	0.35
P1-O1	1.611(7)	1.612(7)	0.06	Al1-O2-P1	158.71(3)	162.65(6)	2.48
P1-O2	1.585(4)	1.587(4)	0.12	Al1-O3-P1	172.13(4)	166.84(3)	-3.07
P1-O3	1.448(5)	1.450(5)	0.14	O1-P1-O1	103.57(3)	103.60(6)	0.03
Al1-(O2)- P1	3.124(1)	3.324(8)	6.45	O1-P1-O2	104.86(2)	104.89(5)	0.03
Al1-(O3)-P1	3.421(5)	3.021(2)	-11.70	O1-P1-O3	108.65(2)	108.88(1)	0.02

References

1 B. Henderson and G. F. Imbusch, *Optical spectroscopy of inorganic solids*, Oxford University Press, 2006.

2 J. H. Nobbs, Kubelka-Munk Theory and the Prediction of Reflectance, *Coloration Technology*, 1985, **15**, 66-75.

3 M. H. Fang, P. Y. Huang, Z. Bao, N. Majewska, T. Leśniewski, S. Mahlik, M. Grinberg, G. Leniec, S. M. Kaczmarek, C. W. Yang, K. M. Lu, H. S. Sheu and R. S. Liu, Penetrating Biological Tissue Using Light-Emitting Diodes with a Highly Efficient Near-Infrared $ScBO_3$:Cr^{3+} Phosphor, *Chem. Mater.*, 2020, **32**, 2166-2171.

4 H. D. Qiyue Shao, Leqi Yao, Junfeng Xu, Chao Liang and Jianqing Jiang, Photoluminescence properties of a $ScBO_3$:Cr^{3+} phosphor and its applications for broadband nearinfrared LEDs., *RSC Advances*, 2018, **8**, 12035-12042.

5 Y. Zhou, S. Yi, Z. Fang, J. Lu, Z. Hu, W. Zhao and Y. Wang, Research on a new type of near-infrared phosphor Li_2MgZrO_4:Cr^{3+}-synthesis, crystal structure, photoluminescence and thermal stability, *Opt. Mater.*, 2021, **117**, 111209.

6 J. Zhong, Y. Zhuo, F. Du, H. Zhang, W. Zhao and J. Brgoch, Efficient and Tunable Luminescence in $Ga_{2-x}In_xO_3$:Cr^{3+} for Near-Infrared Imaging, *ACS Appl. Mater. Interfaces*, 2021, **13**, 31835-31842.

7 M.-H. Fang, K.-C. Chen, N. Majewska, T. Leśniewski, S. Mahlik, G. Leniec, S. M. Kaczmarek, C.-W. Yang, K.-M. Lu, H.-S. Sheu and R.-S. Liu, Hidden Structural Evolution and Bond Valence Control in Near-Infrared Phosphors for Light-Emitting Diodes, *ACS Energy Lett.*, 2021, **6**, 109-114.

8 F. Zhao, H. Cai, Z. Song and Q. Liu, Structural Confinement for Cr^{3+} Activators toward Efficient Near-Infrared Phosphors with Suppressed Concentration Quenching, *Chem. Mater.*, 2021, **33**, 3621-3630.
9 Q. Zhang, D. Liu, P. Dang, H. Lian, G. Li and J. Lin, Two Selective Sites Control of Cr^{3+}-Doped ABO_4 Phosphors for Tuning Ultra-Broadband Near-Infrared Photoluminescence and Multi-Applications, *Laser Photonics Rev.*, 2021, **8**, 2100459.
10 Q. Lin, Q. Wang, M. Liao, M. Xiong, X. Feng, X. Zhang, H. Dong, D. Zhu, F. Wu and Z. Mu, Trivalent Chromium Ions Doped Fluorides with Both Broad Emission Bandwidth and Excellent Luminescence Thermal Stability, *ACS Appl. Mater. Interfaces*, 2021, **13**, 18274-18282.
11 X. Xu, Q. Shao, L. Yao, Y. Dong and J. Jiang, Highly efficient and thermally stable Cr^{3+}-activated silicate phosphors for broadband near-infrared LED applications, *Chem. Eng. J.*, 2020, **383**, 123108.
12 D. Liu, G. Li, P. Dang, Q. Zhang, Y. Wei, H. Lian, M. Shang, C. C. Lin and J. Lin, Simultaneous Broadening and Enhancement of Cr^{3+} Photoluminescence in $LiIn_2SbO_6$ by Chemical Unit Cosubstitution: Night-Vision and Near-Infrared Spectroscopy Detection Applications, *Angew. Chem. Int. Ed. Engl.*, 2021, 202103612.
13 G. Liu, T. Hu, M. S. Molokeev and Z. Xia, Li/Na substitution and Yb^{3+} co-doping enabling tunable near-infrared emission in $LiIn_2SbO_6$:Cr^{3+} phosphors for light-emitting diodes, *iScience*, 2021, **24**, 102250.
14 T. Liu, H. Cai, N. Mao, Z. Song and Q. Liu, Efficient near-infrared pyroxene phosphor $LiInGe_2O_6$:Cr^{3+} for NIR spectroscopy application, *J. Am. Ceram. Soc.*, 2021, 17856.
15 Z. L. Peng Sun, Zhaohua Luo, Rui Dong, and Jun Jiang, Efficient and Broadband $LiGaP_2O_7$:Cr^{3+} Phosphors for Smart Near-Infrared Light-Emitting Diodes, *Laser Photonics Rev.* , 2021, **15**, 202100227.
16 Q. S. Leqi Yao, Shouyu Han, Chao Liang, Jinhua He, and Jianqing Jiang, Enhancing Near-Infrared Photoluminescence Intensity and Spectral Properties in Yb^{3+} Codoped $LiScP_2O_7$:Cr^{3+}, *Chem. Mater.*, 2020, **32**, 2430-2439.
17 S. Miao, Y. Liang, Y. Zhang, D. Chen and X. J. Wang, Broadband Short-Wave Infrared Light-Emitting Diodes Based on Cr^{3+}-Doped $LiScGeO_4$ Phosphor, *ACS Appl. Mater. Interfaces*, 2021, **13**, 36011-36019.
18 H. Cai, S. Liu, Z. Song and Q. Liu, Tuning luminescence from NIR-I to NIR-II in Cr^{3+}-doped olivine phosphors for nondestructive analysis, *J. Mater. Chem. C*, 2021, **9**, 5469-5477.
19 T. Gao, W. Zhuang, R. Liu, Y. Liu, C. Yan and X. Chen, Design of a Broadband NIR Phosphor for Security-Monitoring LEDs: Tunable Photoluminescence Properties and Enhanced Thermal Stability, *Cryst. Growth Des.*, 2020, **20**, 3851-3860.
20 F. Zhao, Z. Song, J. Zhao and Q. Liu, Double perovskite $Cs_2AgInCl_6$:Cr^{3+}: broadband and near-infrared luminescent materials, *Inorg. Chem. Front.*, 2019, **6**, 3621-3628.
21 L. Zhang, D. Wang, Z. Hao, X. Zhang, G. h. Pan, H. Wu and J. Zhang, Cr^{3+}-Doped Broadband NIR Garnet Phosphor with Enhanced Luminescence and its Application in NIR Spectroscopy, *Adv. Optical Mater.*, 2019, **7**, 1900185.
22 V. Rajendran, M. H. Fang, G. N. D. Guzman, T. Lesniewski, S. Mahlik, M. Grinberg, G. Leniec, S. M. Kaczmarek, Y. S. Lin, K. M. Lu, C.-M. Lin, H. Chang, S. F. Hu and R. S. Liu, Super Broadband Near-Infrared Phosphors with High Radiant Flux as Future Light Sources for Spectroscopy Applications, *ACS Energy Lett.*, 2018, **3**, 2679-2684.
23 T. Gao, W. Zhuang, R. Liu, Y. Liu, C. Yan, J. Tian, G. Chen, X. Chen, Y. Zheng and L. Wang, Site occupancy and enhanced luminescence of broadband NIR gallogermanate phosphors by energy transfer, *J. Am. Ceram. Soc.*, 2020, **103**, 202-213.
24 H. Zeng, T. Zhou, L. Wang and R. J. Xie, Two-Site Occupation for Exploring Ultra-Broadband Near-Infrared Phosphor—Double-Perovskite La_2MgZrO_6:Cr^{3+}, *Chem. Mater.*, 2019, **31**, 5245-5253.
25 D. Hou, H. Lin, Y. Zhang, J.-Y. Li, H. Li, J. Dong, Z. Lin and R. Huang, A broadband near-infrared phosphor $BaZrGe_3O_9$:Cr^{3+}: luminescence and application for light-emitting diodes, *Inorg. Chem. Front.*, 2021, **8**, 2333-2340.